communications earth & environment

Article

A Nature Portfolio journal

https://doi.org/10.1038/s43247-026-03362-w

Deoxygenation in the equatorial Panthalassan Ocean predated the end-Triassic mass extinction

Kayla E. McCabe[1,2] ✉, Selva M. Marroquín[2], Andrew H. Caruthers[3], Jeremy D. Owens[4], Martyn L. Golding[5], Rachel E. B. Reid[1,6], Theodore R. Them II[7], João P. Trabucho-Alexandre[8], Yorick P. Veenma[9] & Benjamin C. Gill[1,6]

The end-Triassic mass extinction was one of Earth's largest biotic crises, and marine deoxygenation has been proposed as a primary driver. However, the timing, geographic extent, and severity of oxygen loss in the oceans remain uncertain. Here we present a multi-geochemical proxy record study from the equatorial Panthalassan Ocean that uses sedimentary iron speciation and nitrogen isotopes to reconstruct water column redox changes before, during, and after the mass extinction. Iron speciation data indicate anoxic bottom waters dominated this region through the Late Triassic-Early Jurassic, consistent with deposition beneath an oxygen minimum zone. Elevated nitrogen isotope values ~ 8 million years before the mass extinction record, enhanced denitrification linked to shoaling and expansion of this oxygen minimum zone. These results suggest that deoxygenation in the equatorial Panthalassa began well before the main extinction and coincided with biodiversity declines and carbon-cycle perturbations, likely stressing marine ecosystems before the end-Triassic mass extinction.

The latest Triassic contains one of the most severe mass extinctions in the history of the planet, the End-Triassic Mass Extinction (ETME), that occurred just before the Triassic-Jurassic Boundary (~201 Ma). This event resulted in an ~ 60% loss of marine invertebrates on the generic level[1] and coincided with many paleoenvironmental disturbances[2]. Large-scale volcanism from the Central Atlantic Magmatic Province (CAMP) has been hypothesized to have driven the environmental changes that led to the ETME. These include climatic warming, ocean acidification[3], and deoxygenation[4–9], among others. It has also been suggested more recently that environmental deterioration and extinction rates started to increase well before the ETME, near the Norian-Rhaetian Stage Boundary (NRB)[10]. Although the emplacement of CAMP[11,12] is widely considered to be the primary driver[13,14] of environmental change during the ETME, there is no consensus on the mechanisms behind the events near the NRB.

Marine deoxygenation has been invoked as one of the primary drivers of the ETME[4–9], however the spatiotemporal record of deoxygenation during this interval is not well constrained. Uranium isotope excursions in marine carbonates deposited just after the ETME, near the beginning of the Early Jurassic Hettangian Stage, suggest a 40–100-fold increase in the global extent of anoxic seafloor deposition[15]. Similarly, a sulfate sulfur isotope excursion identified from the latest Rhaetian has been interpreted to indicate a 5-fold increase pyrite burial in anoxic marine sediments[7]. These records are restricted to strata deposited immediately before, during, and shortly after the ETME, meaning the longer-term global history of marine oxygen variability (well) before and (well) after the ETME is largely unknown. Additionally, these proxies i) are only sensitive to anoxic conditions and do not reflect lesser levels of deoxygenation[16–18], and ii) they do not resolve local to regional variations in oxygenation that would strongly influence biotic responses in these marine environments.

Local redox proxies complement these global datasets, but they are largely confined to sedimentary successions from the western Tethys Ocean[4–6,8,9,19,20]. The hydrography of these restricted seaways—characterized by relatively shallow depths, continental proximity, and limited circulation—makes it difficult to extrapolate local occurrences of anoxia to conditions

[1]Department of Geosciences, Virginia Polytechnic Institute and State University, Blacksburg, VA, USA. [2]Department of Geoscience, University of Wisconsin-Madison, Madison, WI, USA. [3]Department of Geological and Environmental Sciences, Western Michigan University, Kalamazoo, MI, USA. [4]Department of Earth, Ocean and Atmospheric Science, National High Magnetic Field Laboratory, Florida State University, Tallahassee, FL, USA. [5]Geological Survey of Canada, Pacific Division, Vancouver, BC, Canada. [6]Global Change Center, Virginia Polytechnic Institute and State University, Blacksburg, VA, USA. [7]Department of Geology and Environmental Geosciences, College of Charleston, Charleston, SC, USA. [8]Department of Earth Sciences, Universiteit Utrecht, Utrecht, TC, The Netherlands. [9]Department of Earth Sciences, University of Cambridge, Cambridge, UK. ✉e-mail: kemccabe3@wisc.edu

in the open oceans. Furthermore, these records share many of the same limitations as the global uranium- and sulfate sulfur isotope datasets, being confined temporally to the interval immediately surrounding the ETME and primarily reflect conditions of full anoxia rather than lesser degrees of oxygen loss[21].

All these factors concerning the marine redox records of the ETME limit our understanding of the history of deoxygenation associated with this event and subsequently its local biotic implications. To address this, we explore a long-term (upper Norian to Hettangian) record of deoxygenation in the understudied equatorial Panthalassic or Panthalassan Ocean using a combination of nitrogen isotope ($\delta^{15}N$) and iron speciation data from Grotto Creek, a sedimentary succession located within the Wrangell Mountains of modern south-central Alaska.

This dual proxy approach is particularly powerful as it permits reconstruction of redox conditions in different portions of the water column[21,22] in this region of Panthalassa. The isotopic composition of bioavailable nitrogen reflects biological and redox processes operating throughout the water column, particularly denitrification within oxygen minimum zones, and is recorded through assimilation into organic matter in the euphotic zone[23,24]. Therefore, $\delta^{15}N$ of sedimentary organic matter provides an avenue to reconstruct changes in the local nitrogen cycling and redox. Iron speciation can be used to distinguish oxic and anoxic conditions within bottom waters using the ratio of highly reactive iron (Fe_{HR}) to the total iron (Fe_T) within sedimentary samples. Likewise, the ratio of pyrite iron to highly reactive iron (Fe_{PY}/Fe_{HR}) can be used to further elucidate whether anoxic bottom waters were ferruginous or euxinic (anoxic and sulfidic water column)[25].

The geochemical records from Grotto Creek reflect the history of nitrogen cycling and water column redox during the Late Triassic and Early Jurassic in east-central Panthalassa. Nitrogen isotopes indicate a shift from nitrate-replete surface waters to progressively more deoxygenated conditions, with increasing denitrification associated with local OMZ expansion beginning in the late Norian and intensifying into the Rhaetian. Notably, these changes in upper water column deoxygenation began well before the ETME. Persistent deoxygenation and denitrification during and after the ETME led to nitrate drawdown and culminated in nitrogen limitation with dominantly anoxic bottom waters. These bottom water conditions were increasingly euxinic during and immediately after the ETME. These conditions continued into Hettangian but were interrupted by a transient oxygenation event marking the first local evidence of environmental recovery after the ETME.

Geologic and paleoenvironmental setting of the Grotto Creek succession

The section at Grotto Creek exposes the McCarthy Formation that consists of Upper Triassic (Norian) to Lower Jurassic (Pliensbachian) strata that were deposited on the Wrangellia Terrane along eastern Panthalassa in a deep-water setting[26–31]. Chronostratigraphic control for the Grotto Creek succession is provided by previously reported biostratigraphy (ammonite, conodont, bivalve, and hydrozoan) and U–Pb zircon dates from interbedded volcanic ash beds (Figs. 1 and 2)[26,27]. Biostratigraphic data from a number of fossil groups from the section base to 4.15 m indicate a late Norian Cordilleranus Zone age. The NRB is placed at 4.15 m in the section defined by the lowest in situ occurrence of *Agerchlamys boellingi* and the Rhaetian ammonoid *Vandaites cf. suttonensis*[27]. Two key ash horizons from 0 and 11.07 m in the section yielded dates of 209.86 ± 0.16 Ma and 208.25 ± 0.25 Ma respectively, temporally constraining the NRB to ~209 Ma[27]. The Triassic-Jurassic Boundary is constrained to the interval of 29.42–33.95 m bounded by the first appearance of the ammonites ?*Psiloceras* sp. and *Psiloceras tilmanni*[27]. The rest of the section studied here (up to 70 m) is Hettangian in age based on the occurrence of ammonites and bivalves (see ref. 27 for further details).

The McCarthy Formation at Grotto Creek is primarily composed of fine-grained limestones and shales (Fig. 2). These strata reflect distal sedimentation of a carbonate ramp deposited off the Wrangellia terrane. The sediment deposited at the Grotto Creek site was sourced from adjacent

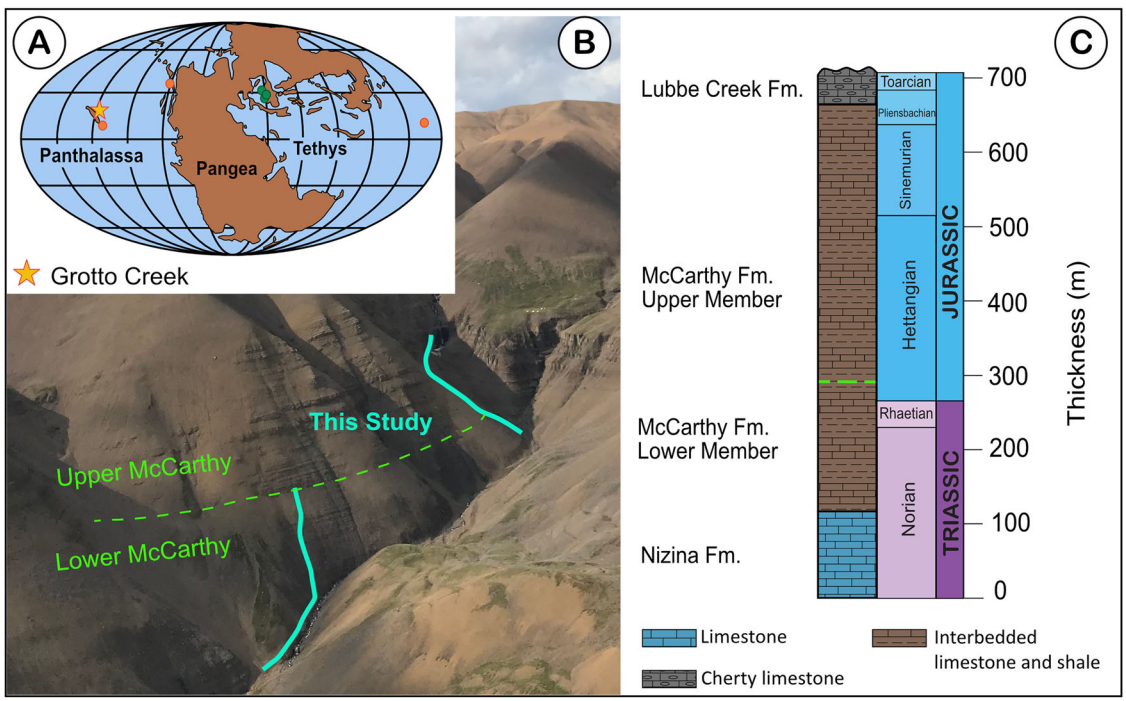

Fig. 1 | Paleogeography of the Late Triassic and stratigraphic setting of the Grotto Creek Section. A Late Triassic global paleogeographic reconstruction displaying the depositional location of the McCarthy Formation[27] (gold star) on the Wrangellia terranes and other known nitrogen isotope records during the ETME (green and orange circles). **B** Aerial photo taken of the Grotto Creek Section with the boundary between the upper and lower McCarthy Formations denoted with the dashed line and the studied sections denoted with the solid blue line. The white dots on the green meadow above the cliff on the middle right of the photo are tents that are 1 meter tall for scale. **C** General stratigraphy of the Grotto Creek Section showing relevant study interval in blue[26–28].

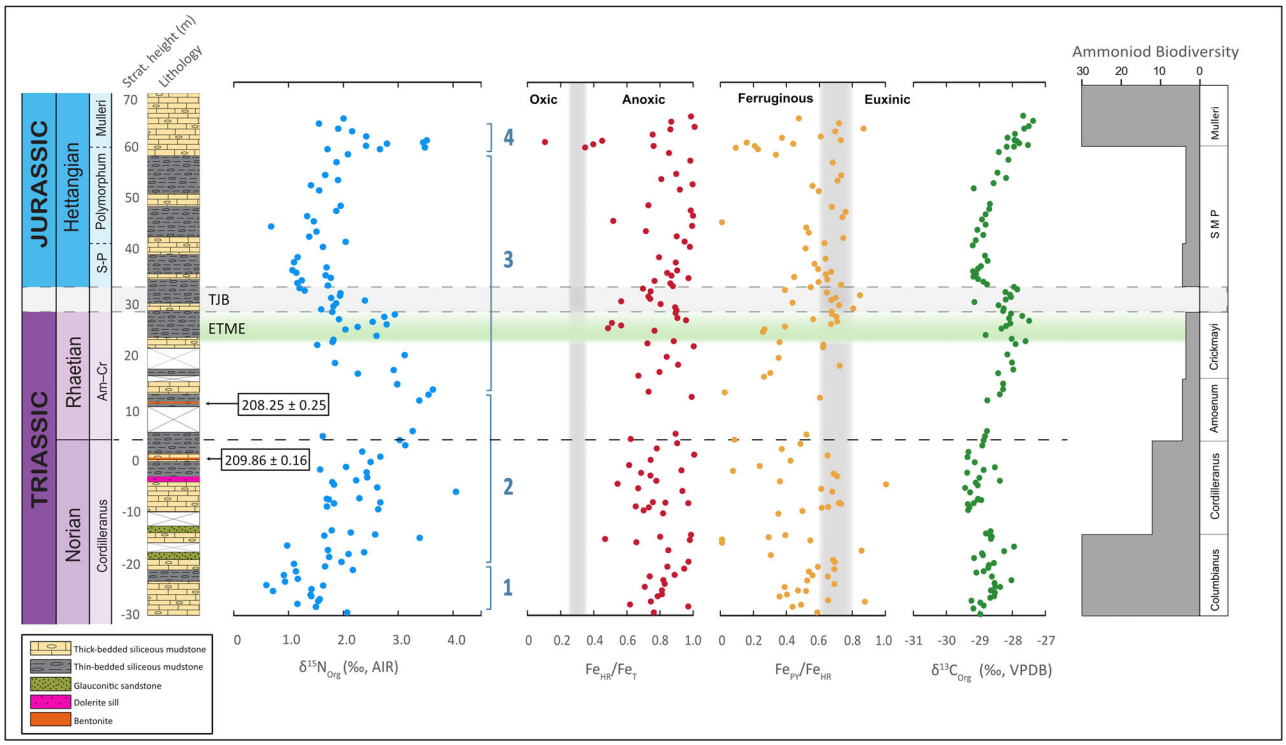

Fig. 2 | Geochemical data spanning the Norian-Rhaetian and End-Triassic Mass Extinction at Grotto Creek, Alaska, USA. Stratigraphic plots of nitrogen isotope and iron speciation proxy data from Grotto Creek displayed with the previously established biostratigraphic, geochronologic, and lithologic framework[22] along with the generic ammonoid biodiversity curve from eastern Panthalassa sites[50]. Nitrogen isotopes are depicted in blue, Fe_{HR}/Fe_T in red, Fe_{PY}/Fe_{HR} in yellow, and organic carbon isotopes[27] in green. Thresholds for Fe speciation[56] are displayed as vertical dashed lines in both the Fe_{HR}/Fe_T (oxic <0.38 <anoxic) and Fe_{PY}/Fe_{HR} (ferruginous <0.6, 0.8 <euxinic) plots. Ash bed dates[27] are shown next to the corresponding stratigraphic height of the sampled bentonite. The stratigraphic interval that contains the Triassic-Jurassic boundary interval is the gray shaded bar whereas the interval that contains the ETME is displayed as the green shaded bar (the base of which is placed at the small negative carbon isotope excursion that occurs below the TJB (referred to as the initial isotope excursion in some references) and the top of which is beneath the first appearance of *Psiloceras tilmanni*).

shallower-water carbonate and siliceous environments and local pelagic sedimentation[28]. The section records a shift to more siliceous sedimentation in the Hettangian[27,28], and this change in the wake of the ETME is noted in many Panthalassan successions that likely reflects the decline of carbonate-producing biota and the proliferation of silica-secreting biota after the extinction[28,32,33].

Results and discussion

Nitrogen isotope and iron speciation results

Two positive $\delta^{15}N$ excursions are observed in the Triassic–Jurassic succession at Grotto Creek, and we interpret these stratigraphic changes in the nitrogen isotopes as reflecting changes in the marine nitrogen cycle (see Supplementary Fig. 1 and Supplementary Discussion for consideration of potential alteration of the nitrogen isotopes). The first is a stratigraphically broad ~+3‰ excursion that extends from the middle of the Norian interval of the Grotto Creek section into the Rhaetian interval. The pre-excursion $\delta^{15}N$ values in this upper Norian part of the section (−30 to −20 m) range from ~+0.5 to +2‰. Above this, between −20 to 0 m, $\delta^{15}N$ values increase to +1.5–3‰ and then continue to rise, reaching their highest values (+3–3.7‰) at ~15 m in the Rhaetian shortly after the NRB. These elevated $\delta^{15}N$ values persist from 0 to 30 m before declining to +1–2‰ across the stratigraphic interval that contains end-Triassic mass extinction and into the Hettangian. The second positive $\delta^{15}N$ excursion of ~3.5‰ occurs between 60-65 m in the Hettangian.

Iron speciation data from throughout the section, save for a brief stratigraphic interval in the Hettangian, have Fe_{HR}/Fe_T values consistently above the 0.38 threshold (average ~0.83) that indicates anoxic bottom water conditions[34]. The Fe_{PY}/Fe_{HR} values vary throughout the section but are generally below 0.6, indicating ferruginous conditions in the water column. Some samples that exceed 0.6 and occasionally 0.8 occur, suggesting euxinia. There is a higher concentration of these euxinic samples between ~25 and 40 m, including the interval that contains the ETME. In the upper part of the section (60 to 65 m), coincident with the second positive $\delta^{15}N$ excursion, Fe_{HR}/Fe_T values decline, with one sample falling below the 0.38 anoxic threshold. At the same time, Fe_{PY}/Fe_{HR} values also drop to near 0. Analyzing a section deposited under persistently reducing bottom-water conditions, as indicated by the iron speciation data, simplifies interpretation of the nitrogen isotope record. In such an environment, stable anoxic conditions would minimize post-depositional alteration of organic nitrogen caused by variable oxygen exposure, microbial oxidation, or differential nitrogen loss and suggest $\delta^{15}N$ values more directly reflect changes in the water-column nitrogen cycle[23].

Regional deoxygenation in equatorial Panthalassa

The geochemical records from Grotto Creek provide insight into the temporal evolution of redox in the upper and lower water column across the Norian–Hettangian interval, including the ETME. Based on the stratigraphic trends in $\delta^{15}N$ that are reflective of redox conditions and nitrogen cycling in the upper water column, we divide the record into four intervals: Interval 1 (−30 to −20 m), contains the upper Norian; Interval 2 (−20 to 13 m), contains the trend to higher $\delta^{15}N$ in the uppermost Norian and into Rhaetian; Interval 3 (13–60 m), captures the variable return to lower $\delta^{15}N$ values through the rest of the Rhaetian into the Hettangian; and Interval 4 (60–65 m), a brief positive $\delta^{15}N$ excursion in the Hettangian. Together, these data indicate dominantly anoxic bottom waters and progressively more reducing upper water-column conditions, and a potential transient shift to less reducing conditions in Interval 4, discussed further below.

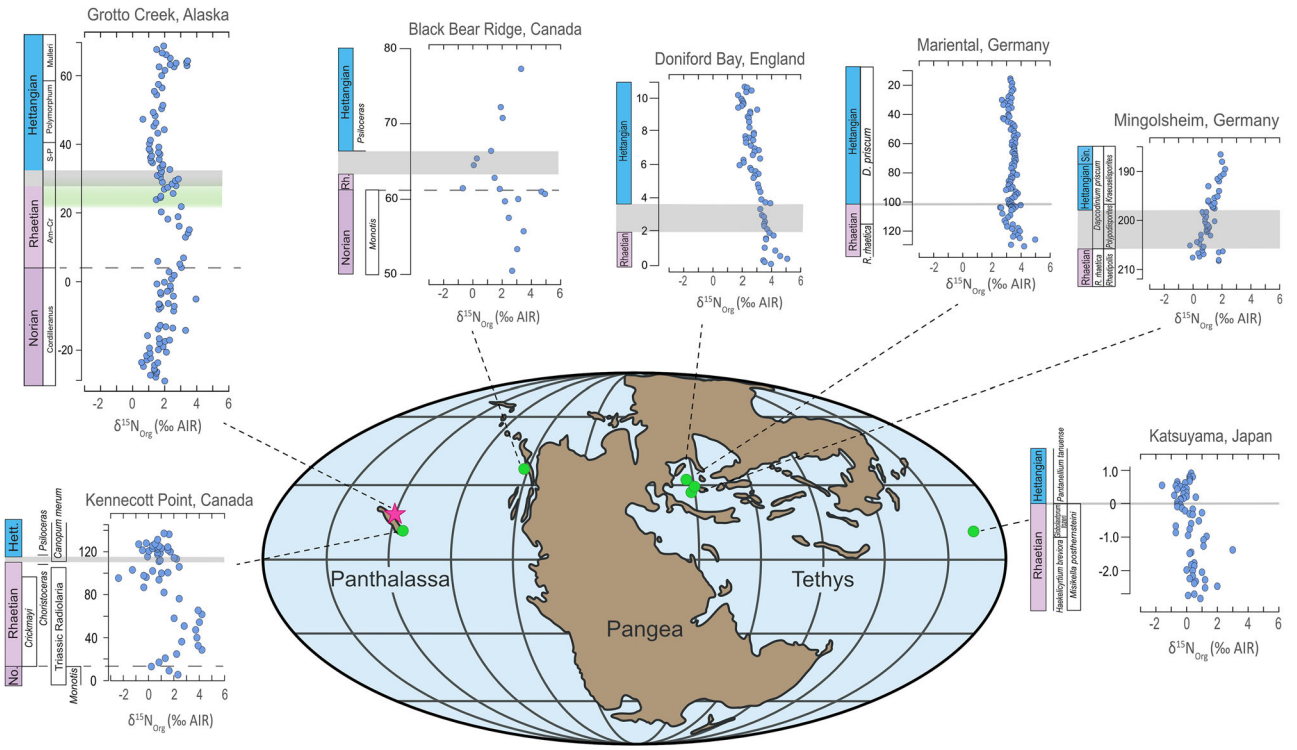

Fig. 3 | Global compilation of nitrogen isotope data from across the latest Triassic-earliest Jurassic. Compilation of nitrogen isotope records across the End-Triassic plotted on a global paleogeographic reconstruction (green circles). Important transitions like the Triassic - Jurassic boundary (highlighted in gray), the Norian - Rhaetian boundary (gray dashed line), and the ETME interval (green shaded zone) are denoted where applicable. Panthalassic study sites include Grotto Creek, Alaska (this study denoted by the star); Kennecott Point, Canada[41]; Black Bear Ridge, Canada[39]; Katsuyama, Japan[45]. Tethys study sites include Doniford Bay, England[64]; Mariental, Germany[5]; Mingolsheim, Germany[4].

In Interval 1 (late Norian), $\delta^{15}N$ values are relatively low (~+0.5–2‰) and co-occur with high (>0.38) Fe_{HR}/Fe_T and variable Fe_{PY}/Fe_{HR}. The nitrogen isotope values are consistent with a scenario in which nitrate was the abundant form of dissolved nitrogen in a well-oxygenated upper water column[35]. Denitrification—if active—was not locally or regionally extensive enough to meaningfully alter the isotopic composition of the nitrate pool[36,37]. Iron speciation data indicate predominantly anoxic, ferruginous, and occasionally euxinic bottom-water conditions. The episodic occurrence of benthic bivalves in this stratigraphic interval[27] may suggest brief intervals of habitable conditions on the seafloor, but the Fe speciation data indicate such intervals were transient. Overall, we interpret this interval to reflect oxygenated surface waters overlying anoxic bottom water conditions, which could represent an OMZ-like scenario.

Interval 2 (latest Norian-middle Rhaetian), containing the NRB, is marked by an increase in $\delta^{15}N$ that peaks at values of +3–3.7‰ that occur with Fe_{HR}/Fe_T>0.38 and variable Fe_{PY}/Fe_{HR}. Iron speciation data display persistently reducing bottom-water conditions, characterized by anoxia that was dominantly ferruginous and intermittently euxinic. The shift to more positive $\delta^{15}N$ suggests increased water-column denitrification that led to enrichment of the residual nitrate pool in ^{15}N and likely reflects the regional expansion of the suboxic zone of the OMZ higher in the water column and closer to the photic zone. This rise in $\delta^{15}N$ initiates in the Norian, indicating that water column deoxygenation increased well before the ETME and persisted into the Rhaetian. These changes in the upper water column coincided with bottom waters that continued to be locally anoxic and variably ferruginous and euxinic (Fig. 2).

Coeval records from elsewhere on Wrangellia and eastern Panthalassa show evidence for a generally similar time-progressive expansion of the regional OMZ. At Kennecott Point (Canada), a positive increase in $\delta^{15}N$ of 3‰ also occurs after the NRB, peaking in the Rhaetian[38] (Fig. 3). Positive $\delta^{15}N$ values similarly occur near the NRB in the succession at Black Bear Ridge (Canada), which was deposited on the western margin of Pangea in eastern Panthalassa[39] (Fig. 3). Although similar in magnitude, these positive $\delta^{15}N$ excursions are slightly diachronous within current dating uncertainties[27,38,39]. We interpret this pattern as reflecting the variable geographic expansion of the regional OMZs before the ETME interval (during the latest Norian and into the Rhaetian).

Interval 3 (middle Rhaetian-to earliest Hettangian including the ETME) is characterized by a variable decline in $\delta^{15}N$ from values more than +3‰ to between +1‰ and +2‰. This was likely caused by prolonged denitrification, which depleted the local marine nitrate reservoir, inducing nitrogen-limited conditions in the surface ocean[23,37]. Under such circumstances, biological nitrogen fixation and/or ammonium recycling likely became dominant sources of bioavailable nitrogen. Both processes would contribute ^{15}N-depleted nitrogen to the organic matter pool, driving the observed decline in $\delta^{15}N$[36,40]. Increased deoxygenation in this interval is supported by the iron speciation data, which indicates continued bottom water anoxia. Notably, the iron speciation data also indicate a higher prevalence of euxinic conditions in and immediately after the interval that contains the ETME.

Other regional Panthalassan records also point to continued deoxygenation and expansion of the OMZ in equatorial Panthalassa during the mid-Rhaetian-to earliest Hettangian. Declines in $\delta^{15}N$ values are observed at Kennecott Point[38] and Black Bear Ridge[39] through the Rhaetian and into the Hettangian, indicating similar changes in the regional nitrogen cycle to those observed at Grotto Creek. Organic biomarker data and redox-sensitive trace metal abundances from Kennecott Point and elsewhere in eastern Panthalassa also indicate the development of bottom-water anoxia and photic zone euxinia during and immediately after the ETME[10,38,41–43].

Interval 4 (early Hettangian) records a second, stratigraphically shorter $\delta^{15}N$ excursion to ~+4‰ in the lowermost Hettangian. This second excursion, although equivalent in magnitude to the excursion preceding the ETME interval, is accompanied by a decrease in both Fe_{HR}/Fe_T and Fe_{py}/Fe_{HR}. These data, taken together, suggest that this $\delta^{15}N$ excursion may

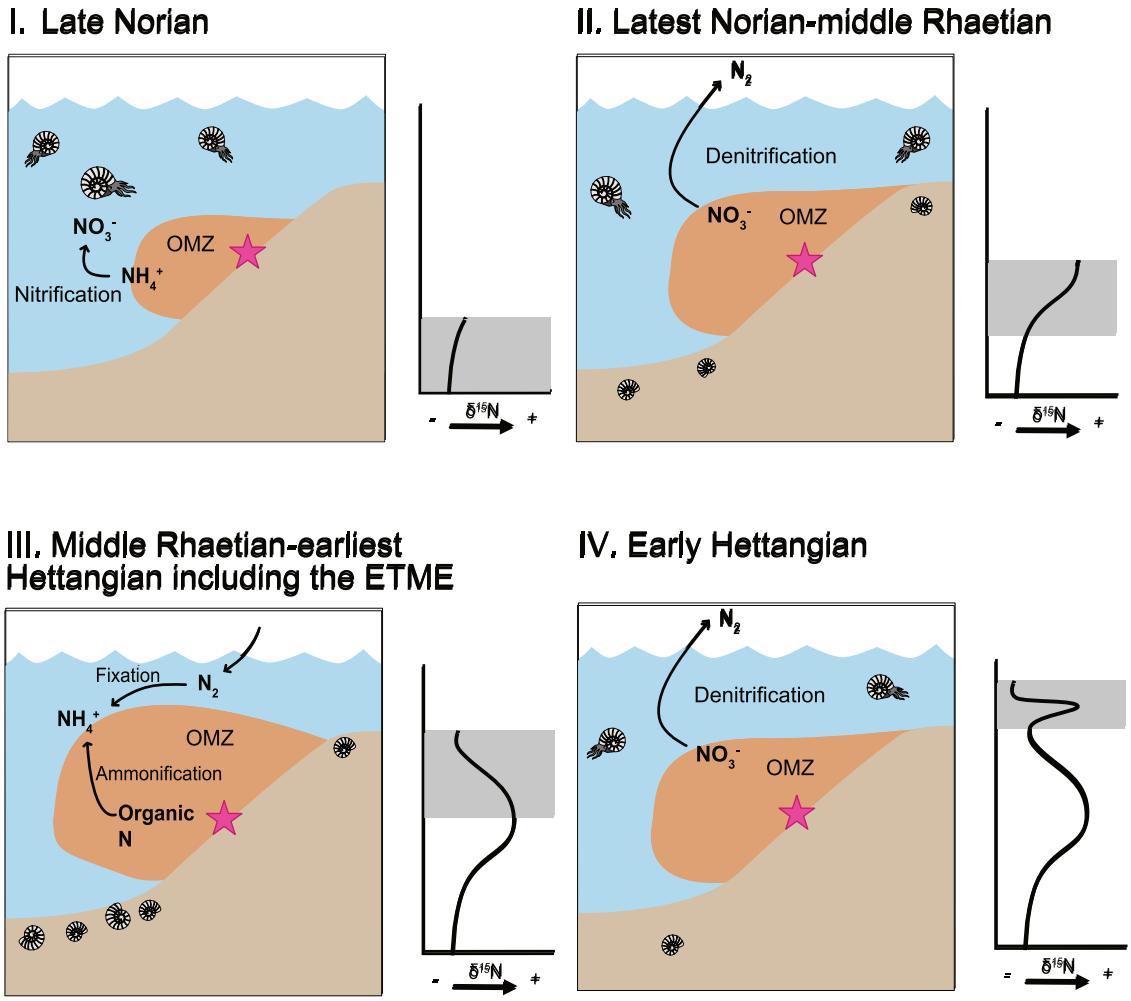

Fig. 4 | Reconstructed history of the equatorial Panthalassan oxygen minimum zone (OMZ) from the Late Triassic to Earliest Jurassic. Nitrogen cycle process indicated are the thought to control the isotope composition of organic nitrogen during each time interval. Pink star indicates the location of Grotto Creek. I). *Late Norian:* Deep oxygen minimum zone (OMZ). Core of OMZ was mostly ferruginous and occasional euxinic. Nitrate is abundant. II.) *Latest Norian-middle Rhaetian*: Expansion of the OMZ. Denitrification starts to deplete the local nitrate pool. Core of OMZ continues to be ferruginous and euxinic. III.) *Middle Rhaetian-to earliest Hettangian including the ETME*: Continued expansion of the OMZ including the into the photic zone. Depletion of the local nitrate pool. Core of OMZ becomes more frequently euxinic. IV.) *Early Hettangian*: OMZ temporarily contracts. Increased nitrate availability. Core of the OMZ returns to being mostly ferruginous and occasional euxinic.

reflect a brief oxygenation event (i.e. less reducing) that generated local suboxic conditions that allowed for the accumulation of nitrate in the surface ocean. This allowed restarting of the partial denitrification of this nitrate pool and the partial ventilation of the lower water column. The transient nature of the $\delta^{15}N$ peak and accompanying changes in the Fe speciation data are consistent with a short-lived event.

Combined, this suggests that the geochemical records from Grotto Creek and other regionally coeval locations reveal a multi-phase evolution of the nitrogen cycle and water column redox during the Late Triassic and Early Jurassic in eastern Panthalassa (Fig. 4). Nitrogen isotopes indicate nitrate-replete surface waters that later experienced deoxygenation and elevated levels of denitrification due to the expansion of the OMZ. Notably, upper-water-column deoxygenation began during the late Norian and intensified into the Rhaetian, well before the ETME. Continued deoxygenation and denitrification led to nitrate drawdown and culminated in nitrogen limitation under bottom-water anoxia and increased occurrence of euxinia during and immediately after the ETME. This continued into the Hettangian but was briefly interrupted by a transient episode of less reducing conditions, which represents the first evidence of localized environmental recovery after the ETME.

The global picture of deoxygenation across the Late Triassic

Multiple lines of evidence indicate that widespread marine deoxygenation occurred across the Late Triassic–Early Jurassic transition. As mentioned above, the uranium isotope redox proxy supports a global expansion of seafloor anoxia during the ETME and its immediate aftermath[15]. While local redox proxy records also broadly support increasing deoxygenation around the ETME and into the Hettangian, these are largely confined to a portion of the western Tethys Ocean. The record from Grotto Creek and other records from northeastern Panthalassa indicate, however, that deoxygenation occurred in this ocean basin well before the ETME (Fig. 4).

Potential evidence for the development of more reducing benthic water column conditions prior to ETME also occurs at other sites farther afield in Panthalassa. Mercury and sulfur enrichments and changes in pyrite framboid morphology in a Japanese deep-sea chert succession deposited in western Panthalassa suggest increases in reducing sedimentary conditions and potentially water column stratification in the Rhaetian some ~1 Myr before the ETME[44,45]. In the Rhaetian portion of a sedimentary succession in western Nevada, the occurrence of goethite replacing pyrite correlated with low macrofaunal abundances has been interpreted reflect sulfidic conditions developing in the local sedimentary pore fluids in east central Panthalassa[46].

Evidence for marine deoxygenation occurring earlier in the Norian and across the NRB outside of Panthalassa remains limited due to a lack of proxy data from this time interval. Recently, a study[43] using redox-sensitive metal abundance data from four globally distributed sites suggested that locally reducing conditions developed in sediments at these locations near the NRB.

More broadly, there is growing evidence for biotic and environmental change in the late Norian and across the NRB. Oxygen isotope evidence points to oceanic warming or changes in evaporation-precipitation dynamics decreasing regional $\delta^{18}O_{sw}$ values in the latest Norian[47,48] that may be related to the expansion of the Panthalassa OMZ. Carbon isotope records from the late Norian and NRB also suggest perturbations to the global carbon cycle[49]. The carbon isotope records at Kennecott Point contain a chaotic carbon interval, consisting of two positive carbon isotope excursions that precede the NRB[49,50]. Further, a global compilation of $\delta^{13}C$ records across the NRB has revealed a negative isotope excursion[10,43]. The $\delta^{13}C$ record from Grotto Creek also displays a negative excursion just below the NRB[27], with the nadir of this excursion occurring near the peak of the $\delta^{15}N$ excursion (Fig. 2). Given the apparent global distribution of the NRB $\delta^{13}C$ excursions, identifying environmental drivers behind them and other coeval geochemical signals should be a priority.

A major decline in ammonoid diversity in eastern Panthalassa occurred in the later Norian[51,52] contemporaneous with the positive $\delta^{15}N$ excursion at Grotto Creek, indicative of enhanced denitrification and deoxygenation within the shallow water column. More broadly, analyses of benthic genera (e.g. bivalves, brachiopods, sponges, corals) globally indicate that 41% of genera crossing the NRB went extinct within the Rhaetian, while at the same time origination rates decreased[53]. These data indicate an overall decrease in marine biodiversity that initiated in the latest Norian, reached a low at the NRB, and remained low during the ETME interval[51,52]. The expansion of the OMZs in the eastern Panthalassa likely played a role in these marine ecosystem crises.

Presently, there is no consensus for triggers of biological crises and geochemical anomalies predating the ETME and CAMP emplacement. The oldest CAMP deposits are ~201.63 Ma[14], which is younger than the NRB at Grotto Creek (~209.8 Ma). Volcanism associated with the Angayucham terrane of southern Alaska, dated at ~214 Ma[53], has previously been considered as a potential trigger for the environmental and biological changes documented at the NRB. However, the large uncertainty associated with this age (± 7 Myr) makes it difficult to determine whether volcanism associated with this terrane was active during the interval of NRB redox change. More precise radiometric constraints are therefore required to better evaluate its potential role. Recently, evidence has been presented for marine large igneous province (LIP) eruptive activity in Tethys Ocean during the late Norian, with age estimates that more closely align with the timing of the NRB[54]. Consistent with this timing, a strontium isotope excursion identified in the latest Norian of eastern Panthalassa may reflect enhanced hydrothermal or volcanic inputs during this interval[55]. Regardless of the driver, the changes in marine biogeochemical processes reflected in the $\delta^{13}C$, $\delta^{15}N$, and iron-speciation records across the NRB appear to have influenced marine ecosystems well before the ETME.

Conclusions

These geochemical datasets from Grotto Creek provide additional insights into marine deoxygenation in equatorial Panthalassa during the Late Triassic to Early Jurassic. The dual nitrogen isotope and iron speciation data presented here allow for the assessment of redox changes in both the shallow and deep portions of the water column. The $\delta^{15}N$ and iron speciation data suggest: (i) progressive deoxygenation in eastern Panthalassa initiated in the late Norian, before the ETME, with the expansion of the local OMZ into shallow waters; (ii) this deoxygenation event coincides not only with known regional and global biodiversity declines in ammonoids and benthic genera (respectively), but also recently discovered perturbations to the global carbon cycle; (iii) these environmental and biologic crises predated CAMP emplacement and the events of the ETME by ~8 Ma. These data, when placed in the context of existing datasets, suggest a progressive and protracted expansion of the OMZ in eastern equatorial Panthalassa. While the underlying drivers of these earlier changes to the Earth system (preceding CAMP and the ETME) are unclear, their effects likely set the stage for the ETME, and a better understanding of them is key to unraveling the full story of this chapter in Earth history.

Methods

Nitrogen isotopes

Samples were powdered and reacted with 5–7 mL of 2 M HCl at room temperature to remove all carbonate (~24–48 h). Sample residues were separated from reacted HCl, rinsed (deionized water was added to the 15 mL sample tubes which were then vortexed to suspend sediments, centrifuged to settle sediments to the bottom of the tubes, and then pH was measured) multiple times until attaining a pH of 5 or higher. Samples were then dried in a 55 °C oven and once dry, re-homogenized into a fine powder using a mortar and pestle. Samples and standards, including USGS 25 (−30.41 ± 0.16 ‰) and USGS 26 (+ 53.75 ± 0.15 ‰) and a commercial low organic soil standard (EA Consumables), were weighed into tin capsules. Isotopic analyses were performed using an Isoprime 100 isotope ratio mass spectrometer (IRMS) with an Elementar vario Isotope Cube elemental analyzer (EA). Nitrogen isotope data were corrected for linearity and drift over the course of the run and then normalized to the AIR scale to determine $\delta^{15}N$ values. Reproducibility of nitrogen isotope analyses can be estimated using replicates of the USGS25 and USGS26 standards run with the samples that yielded standard deviations of 0.21 and 0.26, respectively. The organic total nitrogen content of each sample was determined using the area of the N_2 peak measured by the elemental analyzer calibrated to a size series of low organic soil elemental standards. Nitrogen contents calculated using this method averaged less than 5% error from the known composition of the standards.

Organic carbon isotopes ($\delta^{13}C_{org}$) and total organic carbon content (TOC)

Total organic carbon content (TOC) and isotopic composition ($\delta^{13}C_{org}$) were measured on the same samples residues as the nitrogen isotopes. Decarbonated sample powders (4 to 40 mg) were weighed into tin capsules and combusted at 950 °C in an Elementar Vario Cube elemental analyzer connected to an Isoprime 100 isotope ratio mass spectrometer (IRMS) the stable isotope lab in the Department of Geosciences at Virginia Tech. The isotope compositions of the samples were normalized to the VPDB scale with international and commercial isotopic standards (CH-6 = 10.449‰; CH-7 = 32.151‰; Elemental Microanalysis wheat flour = 27.21‰) run with the samples. The average standard deviation (1σ) of the isotopic standards was <±0.1‰. The TOC contents of the samples were determined using the integrated area of the CO_2 peak measured by thermal conductivity detector in the elemental analyzer that was calibrated to a size series of elemental standards (Elemental Microanalysis acetanilide and wheat flour) elemental standards in each run. The carbon content of the acetanilide and wheat flour standards not included in the calibration series was within 5% of their known compositions. TOC contents of the original samples were determined using the carbon contents of the decarbonated residue adjusted using the ratio of the mass of the decarbonated sample to the original treated bulk powder to account for the mass lost during decarbonation. Carbon and nitrogen isotope data as well as wt% and C:N ratios are provided in Supplementary Table 1 and Supplementary Data.

Iron speciation proxy

The sequential iron extractions used for this study followed the standard method[56]. Briefly, 0.1–0.2 g of sample powder was reacted sequentially with three different reagents used to target specific iron-bearing mineral phases in the rock: (1) 1 M sodium acetate solution buffered to pH 4.5 for 48 h at 50 °C to target iron in carbonate minerals (Fe_{carb}) such as siderite and ankerite; (2) sodium dithionite (50 g/L) solution buffered to pH 4.8 for 2 h to target iron

in oxides and hydroxides (Fe_{ox}) such as goethite and hematite; and (3) 0.2 M ammonium oxalate and 0.17 M oxalic acid buffered to pH of 3.2 for 6 h to target iron in magnetite (Fe_{mag}). After each extraction, iron concentrations in the solutions were quantified by spectrophotometry using the modified version of the ferrozine method[57,58] Replicate sample extractions from each extraction yielded reproducibility better than 7%.

Pyrite iron was extracted using the chromium-reducible sulfur (CRS) extraction[59]. In this method, ~0.1 to 0.3 g of sample powder was reacted with a 1 M chromous chloride solution while being heated for 2 h on a distillation line. The sulfur in pyrite liberated as H_2S gas was sequentially flushed using nitrogen gas into a vessel filled with a zinc acetate solution, precipitating solid ZnS. This ZnS was then converted to Ag_2S by adding $AgNO_3$ solution to the zinc acetate solution with the captured ZnS. The precipitate was dried and weighed to determine the pyrite iron contents (Fe_{py}) by assuming a 2:1 stoichiometric relationship between sulfur and iron from the original pyrite (FeS_2). Recovery of sulfur from pure pyrite, run at the same time as the samples, was within 95% of the expected value. Replicate analyses of the samples via this method were within 5%.

Total iron (Fe_T) contents were determined following a modified version of the method described by Aller et al.[60]. Here, 0.3 g of sample powder was placed in crucibles and heated in a muffle furnace to 900 °C for 6 h. The ashed powders were weighed, homogenized, and placed in sealed Savillex vials with concentrated 12 M HCl, sealed, and heated to 145 °C for 48 h. After this, an aliquot of solution was analyzed to determine its iron content using the ferrozine spectrophotometry method described above, and replicate analyses of the samples were within 5%.

Iron speciation can be used to distinguish oxic and anoxic water column conditions using the ratio of highly reactive iron (Fe_{HR}) to the total iron (Fe_T) within sedimentary samples with $Fe_{HR}/Fe_T < 0.22$ indicative of bottom water deposition under oxic water columns; > 0.38 deposition under anoxic water column; and between 0.22 and 0.38 indicates ambiguous redox during deposition[25,26]. Sediments deposited under an anoxic water column can be further classified based on the proportion of the Fe_{HR} pool found in pyrite (Fe_{py}): $Fe_{py}/Fe_{HR} < 0.6$ indicates an anoxic and iron-rich (ferruginous) water column; and >0.8 is representative of anoxic and sulfidic (euxinic) water column. Fe_{py}/Fe_{HR} values between 0.6 and 0.8 are considered equivocal and could represent deposition under either ferruginous or euxinic water columns[25,61–63]. Iron speciation data are provided in Supplementary Table 2 and Supplementary Data.

Data availability

The geochemical dataset generated for and analysed within this study is available in the Figshare repository, https://doi.org/10.6084/m9.figshare.31286599.

Received: 19 March 2025; Accepted: 24 February 2026;
Published online: 01 April 2026

References

1. Alroy, J. et al. Phanerozoic trends in the global diversity of marine invertebrates. *Science* **321**, 97–100 (2008).
2. Korte, C., Ruhl, M., Pálfy, J., Ullmann, C. V. & Hesselbo, S. P. Chemostratigraphy Across the Triassic–Jurassic Boundary. in *Chemostratigraphy Across Major Chronological Boundariess, Geophysical Monograph* 240 (eds Sial, A. N., Gaucher, C., Ramkumar, M. & Ferreira, V. P.) 183–210 (American Geophysical Union (A. G. U.). https://doi.org/10.1002/9781119382508.ch10 (2019).
3. Greene, S. E. et al. Recognising ocean acidification in deep time: An evaluation of the evidence for acidification across the Triassic-Jurassic boundary. *Earth Sci. Rev.* **113**, 72–93 (2012).
4. Quan, T. M., van de Schootbrugge, B., Field, M. P., Rosenthal, Y. & Falkowski, P. G. Nitrogen isotope and trace metal analyses from the Mingolsheim core (Germany): Evidence for redox variations across the Triassic-Jurassic boundary. *Glob. Biogeochem. Cycles* **22**, n/a-n/a (2008).
5. Richoz, S. et al. Hydrogen sulphide poisoning of shallow seas following the end-Triassic extinction. *Nat. Geosci.* **5**, 662–667 (2012).
6. Jaraula, C. M. B. et al. Elevated pCO_2 leading to Late Triassic extinction, persistent photic zone euxinia, and rising sea levels. *Geology* **41**, 955–958 (2013).
7. He, T. et al. An enormous sulfur isotope excursion indicates marine anoxia during the end-Triassic mass extinction. *Sci. Adv.* **6**, eabb6704 (2020).
8. He, T. et al. Shallow ocean oxygen decline during the end-Triassic mass extinction. *Glob. Planet. Change* **210**, 103770 (2022).
9. He, T. et al. Extensive marine anoxia in the European epicontinental sea during the end-Triassic mass extinction. *Glob. Planet. Change* **210**, 103771 (2022).
10. Rigo, M. et al. The Late Triassic extinction at the Norian/Rhaetian boundary: biotic evidence and geochemical analysis. *Earth Sci. Rev*. 103180 (2020) https://doi.org/10.1016/j.earscirev.2020.103180.
11. Schaller, M. F., Wright, J. D. & Kent, D. V. Atmospheric pCO_2 perturbations associated with the central atlantic magmatic province. *Science* **331**, 1404–1409 (2011).
12. Ruhl, M., Bonis, N. R., Reichart, G.-J., Damste, J. S. S. & Kurschner, W. M. Atmospheric carbon injection linked to end-Triassic mass extinction. *Science* **333**, 430–434 (2011).
13. Blackburn, T. J. et al. Zircon U-Pb geochronology links the end-Triassic extinction with the Central Atlantic Magmatic Province. *Science* **340**, 941–946 (2013).
14. Davies, J. H. F. L. et al. End-Triassic mass extinction started by intrusive CAMP activity. *Nat. Commun.* **8**, 15596 (2017).
15. Jost, A. B. et al. Uranium isotope evidence for an expansion of marine anoxia during the end-Triassic extinction. *Geochem. Geophys. Geosyst.* **18**, 3093–3108 (2017).
16. Owens, J. D. *Application of Thallium Isotopes: Tracking Marine Oxygenation through Manganese Oxide Burial*. https://doi.org/10.1017/9781108688697. (Cambridge University Press, 2019).
17. Lau, K. V., Romaniello, S. J. & Zhang, F. The uranium isotope paleoredox proxy. *Elem. Geochem. Tracers Earth Syst. Sci.* https://doi.org/10.1017/9781108584142 (2019).
18. Bottrell, S. H. & Newton, R. J. Reconstruction of changes in global sulfur cycling from marine sulfate isotopes. *Earth-Sci. Rev.* **75**, 59–83 (2006).
19. Beith, S. J., Fox, C. P., Marshall, J. E. A. & Whiteside, J. H. Recurring photic zone euxinia in the northwest Tethys impinged end-Triassic extinction recovery. *Palaeogeogr. Palaeoclimatol. Palaeoecol.* **584**, 110680 (2021).
20. Fox, C. P. et al. Two-pronged kill mechanism at the end-Triassic mass extinction. *Geology* https://doi.org/10.1130/G49560.1 (2022).
21. Stüeken, E. E., Kipp, M. A., Koehler, M. C. & Buick, R. The evolution of Earth's biogeochemical nitrogen cycle. *Earth-Sci. Rev.* **160**, 220–239 (2016).
22. Zerkle, A. L. et al. Onset of the aerobic nitrogen cycle during the Great Oxidation Event. *Nature* **542**, 465–467 (2017).
23. Robinson, R. S. et al. A review of nitrogen isotopic alteration in marine sediments: N isotopic alteration in marine sediment. *Paleoceanography* **27**, (2012).
24. Mettam, C. & Zerkle, A. L. Nitrogen isotopes in deep time. *Elem. Geochem. Tracers Earth Syst. Sci.* https://doi.org/10.1017/9781108847186 (2021).
25. Poulton, S. W. *The Iron Speciation Paleoredox Proxy*. https://doi.org/10.1017/9781108847148. (Cambridge University Press, 2021).
26. Witmer, J. W. Sedimentology and Stratigraphy of the Upper Triassic - Lower Jurassic McCarthy Formation, Wrangell Mountains, South-Central Alaska. (Bucknell University, 2007).
27. Caruthers, A. H. et al. New evidence for a long Rhaetian from a Panthalassan succession (Wrangell Mountains, Alaska) and regional differences in carbon cycle perturbations at the Triassic-Jurassic transition. *Earth Planet. Sci. Lett.* **577**, 117262 (2022).

28. Veenma, Y. P. et al. The glass ramp of Wrangellia: late Triassic to early Jurassic outer ramp environments of the McCarthy Formation, Alaska. *USA J. Sediment. Res.* **92**, 896–919 (2022).
29. MacKevett, E. M. *Stratigraphy and General Geology of the McCarthy C-5 Quadrangle*, *Alaska*. (U.S. Government Printing Office, 1971).
30. MacKevett, E. M. *Geologic Map of the McCarthy B-5 Quadrangle, Alaska*. *USGS Report* 24 https://ui.adsabs.harvard.edu/abs/1974usgs.rept…24M https://doi.org/10.3133/gq1146 (1974).
31. MacKevett, E. M. Geologic map of the McCarthy Quadrangle, Alaska. IMAP https://doi.org/10.3133/i1032 (1978).
32. Ritterbush, K. A., Rosas, S., Corsetti, F. A., Bottjer, D. J. & West, A. J. Andean sponges reveal long-term benthic ecosystem shifts following the end-Triassic mass extinction. *Palaeogeogr. Palaeoclimatol. Palaeoecol.* **420**, 193–209 (2015).
33. Ritterbush, K. Sponge meadows and glass ramps: state shifts and regime change. *Palaeogeogr. Palaeoclimatol. Palaeoecol.* **513**, 116–131 (2019).
34. Poulton, S. W. & Canfield, D. E. Ferruginous conditions: a dominant feature of the ocean through Earth's history. *Elements* **7**, 107–112 (2011).
35. Stüeken, E. E. et al. Marine biogeochemical nitrogen cycling through Earth's history. *Nat. Rev. Earth Environ.* **5**, 732–747 (2024).
36. Altabet, M. A. & Francois, R. Sedimentary nitrogen isotopic ratio as a recorder for surface ocean nitrate utilization. *Glob. Biogeochem. Cycles* **8**, 103–116 (1994).
37. Scholz, F. Identifying oxygen minimum zone-type biogeochemical cycling in Earth history using inorganic geochemical proxies. *Earth-Sci. Rev.* **184**, 29–45 (2018).
38. Schoepfer, S. D., Algeo, T. J., Ward, P. D., Williford, K. H. & Haggart, J. W. Testing the limits in a greenhouse ocean: Did low nitrogen availability limit marine productivity during the end-Triassic mass extinction. *Earth Planet Sci. Lett.* **451**, 138–148 (2016).
39. Sephton, M. A. et al. Carbon and nitrogen isotope disturbances and an end-Norian (Late Triassic) extinction event. *Geology* **30**, 1119–1122 (2002).
40. Galbraith, E. D. et al. Consistent relationship between global climate and surface nitrate utilization in the western subarctic Pacific throughout the last 500 ka. *Paleoceanography* **23**, (2008).
41. Kasprak, A. H. et al. Episodic photic zone euxinia in the northeastern Panthalassic Ocean during the end-Triassic extinction. *Geology* **43**, 307–310 (2015).
42. Larina, E. et al. Uppermost Triassic phosphorites from Williston Lake, Canada: link to fluctuating euxinic-anoxic conditions in northeastern Panthalassa before the end-Triassic mass extinction. *Sci. Rep.* **9**, 18790 (2019).
43. Rigo, M. et al. Unveiling a new oceanic anoxic event at the Norian/Rhaetian boundary (Late Triassic). *Sci. Rep.* **14**, 15574 (2024).
44. Schoepfer, S. D., Algeo, T. J., van de Schootbrugge, B. & Whiteside, J. H. The Triassic–Jurassic transition – A review of environmental change at the dawn of modern life. *Earth-Sci. Rev.* **232**, 104099 (2022).
45. Fujisaki, W. et al. Redox conditions and nitrogen cycling during the Triassic-Jurassic transition: A new perspective from the mid-Panthalassa. *Earth-Sci. Rev.* **204**, 103173 (2020).
46. Larina, E. et al. Ecosystem change and carbon cycle perturbation preceded the end-Triassic mass extinction. *Earth Planet. Sci. Lett.* **576**, 117180 (2021).
47. Sun, Y. D., Orchard, M. J., Kocsis, ÁT. & Joachimski, M. M. Carnian–Norian (Late Triassic) climate change: Evidence from conodont oxygen isotope thermometry with implications for reef development and Wrangellian tectonics. *Earth Planet. Sci. Lett.* **534**, 116082 (2020).
48. Trotter, J. A., Williams, I. S., Nicora, A., Mazza, M. & Rigo, M. Long-term cycles of Triassic climate change: a new δ18O record from conodont apatite. *Earth Planet. Sci. Lett.* **415**, 165–174 (2015).
49. Zaffani, M. et al. The Norian "chaotic carbon interval": New clues from the δ13Corg record of the Lagonegro Basin (southern Italy). *Geosphere* **13**, 1133–1148 (2017).
50. Whiteside, J. H. & Ward, P. D. Ammonoid diversity and disparity track episodes of chaotic carbon cycling during the early Mesozoic. *Geology* **39**, 99–102 (2011).
51. Whiteside, J. H. et al. Pangean great lake paleoecology on the cusp of the end-Triassic extinction. *Palaeogeogr. Palaeoclimatol. Palaeoecol.* **301**, 1–17 (2011).
52. Lucas, S. G. Late Triassic Ammonoids: Distribution, Biostratigraphy and Biotic Events. in *The Late Triassic World* (ed. Tanner, L. H.) vol. 46 237–261 (Springer, 2018).
53. Kiessling, W., Aberhan, M., Brenneis, B. & Wagner, P. J. Extinction trajectories of benthic organisms across the Triassic–Jurassic boundary. *Palaeogeogr. Palaeoclimatol. Palaeoecol.* **244**, 201–222 (2007).
54. Fan, J.-J. *et al*. Marine large igneous provinces: Key drivers of Triassic recurrent extinction. Geology https://pubs.geoscienceworld.org/gsa/geology/article-standard/doi/10.1130/G53406.1/724643/Marine-large-igneous-provinces-Key-drivers-of (2026).
55. Clement, A. M., Tackett, L. S. & Marolt, S. Biosediment assemblages reveal disrupted silica cycling and redox conditions throughout the Rhaetian Stage: Evidence for a precursor event to the end-Triassic mass extinction. *Palaeogeogr. Palaeoclimatol. Palaeoecol.* **638**, 112034 (2024).
56. Poulton, S. W. & Canfield, D. E. Development of a sequential extraction procedure for iron: implications for iron partitioning in continentally derived particulates. *Chem. Geol.* **214**, 209–221 (2005).
57. Stookey, L. L. Ferrozine–a new spectrophotometric reagent for iron. *Anal. Chem.* **42**, 779–781 (1970).
58. Viollier, E., Inglett, P. W., Hunter, K., Roychoudhury, A. N. & Van Cappellen, P. The ferrozine method revisited: Fe(II)/Fe(III) determination in natural waters. *Appl. Geochem.* **15**, 785–790 (2000).
59. Canfield, D. E., Raiswell, R., Westrich, J. T., Reaves, C. M. & Berner, R. A. The use of chromium reduction in the analysis of reduced inorganic sulfur in sediments and shales. *Chem. Geol.* **54**, 149–155 (1986).
60. Aller, R. C., Mackin, J. E. & Cox, R. T. Diagenesis of Fe and S in Amazon inner shelf muds: apparent dominance of Fe reduction and implications for the genesis of ironstones. *Cont. Shelf Res.* **6**, 263–289 (1986).
61. Anderson, T. F. & Raiswell, R. Sources and mechanisms for the enrichment of highly reactive iron in euxinic Black Sea sediments. *Am. J. Sci.* **304**, 203–233 (2004).
62. Benkovitz, A. et al. Tracing water column euxinia in Eastern Mediterranean Sapropels S5 and S7. *Chem. Geol.* **545**, 119627 (2020).
63. Raiswell, R. et al. The iron paleoredox proxies: A guide to the pitfalls, problems and proper practice. *Am. J. Sci.* **318**, 491–526 (2018).
64. Paris, G. et al. Nitrogen isotope record of a perturbed paleoecosystem in the aftermath of the end-Triassic crisis, Doniford section, SW England. *Geochem. Geophys. Geosystems* **11**, (2010).

Acknowledgements

We gratefully acknowledge the support for this study from United States National Science Foundation grant EAR-2026926 to B.C.G., A.H.C., and J.D.O. We also thank the Virginia Tech College of Science Dean's Discovery Fund grant to BCG and National Geographic Society (NGS-9973-16) to AHC for financial support of the fieldwork. We thank the field crew who braved the Alaskan wilderness in 2017 and 2019 to collect samples that were instrumental to this work. We also thank Paul Claus and Ultima Thule Lodge for air support and National Park Service and Wrangell–St. Elias National Park and Preserve for access to the Grotto Creek site. The samples for this research were collected under research and collecting permits WRST-2017-SCI0004 and WRST-2018-SC1-0005. Finally, we thank the Communications Earth & Environment editors for handling our manuscript, as well as Dr. Shane

Schoepfer and two anonymous reviewers for their constructive feedback that help improve our manuscript.

Author contributions

K.E.M. conceived and designed the study, collected geochemical data, processed data, interpreted results, and led manuscript writing. S.M.M. conducted fieldwork, contributed to iron speciation acquisition, and contributed to manuscript review and editing. A.H.C. conducted fieldwork, developed the ammonoid biostratigraphic framework, contributed to manuscript review and editing, and acquired funding. J.D.O. conducted fieldwork, contributed to manuscript review and editing, and acquired funding. M.L.G. conducted fieldwork, contributed to manuscript review and editing, and provided conodont biostratigraphic and preservation expertise. R.E.R. supervised and assisted with nitrogen isotope analyses, contributed to data processing, and participated in manuscript review and editing. T.R.T. conducted fieldwork and contributed to manuscript review and editing. J.P.T.-A. conducted fieldwork, led stratigraphic description, and participated in manuscript review and editing. Y.P.V. conducted fieldwork, contributed to lithologic and sedimentologic descriptions, and participated in manuscript review and editing. B.C.G. contributed to study conception and design, supervised the project, contributed to carbon isotope and iron speciation data acquisition, interpreted results, acquired funding, and contributed to manuscript writing and editing. All authors discussed the results and approved the final manuscript.

Competing interests

The authors declare no competing interests.

Additional information

Supplementary information The online version contains supplementary material available at https://doi.org/10.1038/s43247-026-03362-w.

Correspondence and requests for materials should be addressed to Kayla E. McCabe.

Peer review information *Communications Earth and Environment* thanks the anonymous reviewers for their contribution to the peer review of this work. Primary Handling Editors: Jun Shen and Martina Grecequet. [A peer review file is available].